Journal of Non-Crystalline Solids 427 (2015) 41–45

Contents lists available at ScienceDirect

Journal of Non-Crystalline Solids

journal homepage: www.elsevier.com/ locate/ jnoncrysol

Hexagonal nanosheets in amorphous BN: A first principles study

Murat Durandurdu

Department of Materials Science & Nanotechnology Engineering, Abdullah Gül University, Kayseri 38039, Turkey

ARTICLE INFO

Article history:
Received 29 April 2015
Received in revised form 13 July 2015
Accepted 15 July 2015
Available online 21 July 2015

Keywords:
Boron nitride;
Nanosheet;
Amorphous

ABSTRACT

Amorphous boron nitrite is modeled by means of first principles molecular dynamics simulations and found to be almost chemically ordered in a stark contrast to the previous predictions. Its average coordination number is 2.97. The main building unit of the amorphous network is hexagonal rings as in the most stable boron nitrite phase but chain-like structures and tetragonal-like rings also exist in amorphous network. The model consists of partially hexagonal nanosheets and hence it is not entirely disordered. Amorphous boron nitrite has a band gap energy of about 2.0 eV.

1. Introduction

Boron nitride (BN) can have both amorphous and crystalline phases at ambient and high pressure and temperature conditions. The hexagonal BN (*h*-BN) is the most stable phase having a two-dimensional layered structure, similar to graphite [1]. In the layers, B and N atoms form interconnecting hexagonal rings and the B—N bonding is very strong (covalent) but the layers are held together by the weak Van der Waals forces. Therefore *h*-BN can be easily compressible under stress. Rhombohedral BN (*r*-BN) is another two-dimensional form of BN consisting of a stacking arrangement of three layers [2]. Cubic BN (*c*-BN), a three-dimensional form, exists in the zinc-blende structure and can be easily synthesized from *h*-BN at high temperature and pressure conditions [3]. *c*-BN is tetrahedrally bonded and an extremely hard material. BN can also crystallize in the wurtzite structure (*w*-BN) that can be produced by annealing *h*-BN at high temperatures and pressures as well [4]. Analogous to *c*-BN, *w*-BN is also tetrahedrally coordinated and is a candidate for superhard materials. When amorphous BN (*a*-BN) is considered, regrettably, its atomic structure and properties are not as clear as those of the crystalline phases in spite of numerous investigations [5–19]. Since the physical, chemical, mechanical and electronic properties of *a*-BN will correlate with its bonding natures, it is truly important to have an atomistic level description of *a*-BN to understand its properties in details and to outline its possible technological applications.

It was reported that the amorphous sample prepared by a ball milling technique [8] and hydrogenated *a*-BN synthesized by very high frequency plasma chemical vapor deposition [7] consisted of mainly sp^2 bonding but they also had a small amount of sp^3 bonding. On the other hand, simulations [18,19] offered strikingly different pictures for *a*-BN. Amorphous models generated using an ab initio method [19] exhibited N_2 dimers and a noticeable amount of homopolar (wrong or like) bonds. *a*-BN with various densities was created using density-functional tight binding simulations [18] and similar to the ab initio prediction, the formation of N_2 dimers and B—B and N—N wrong bonds was observed in each model. Interestingly the average B—B coordination number was found to be roughly two and independent of the density of the models [18]. To our knowledge, the presence of homopolar bonds in *a*-BN has not been discussed in any experiment except in boron-rich amorphous films [20]. This might imply that it is chemically ordered or has a negligible amount of homopolar bonds. Too short simulation time (less than a few picosecond) used in these theoretical approaches [18,19] is possibly the main reason for the presence of many dimers, which is, we believe, also responsible for a great number of homopolar bonds in the computer generated models.

The main objective of the present study is to model a realistic *a*-BN network using an ab initio technique and to uncover its properties that have not been revealed in the previous investigations so far. Our findings suggest a nearly chemically ordered model in which sp^2 bonding is dominated and produces largely hexagonal and tetragonal rings. The *a*-BN model is found to be a mixture of nanoscale hexagonal and amorphous phases.

2. Method

The simulation was performed using SIESTA ab initio code [21] that is based on first principles density functional theory (DFT). A double-zeta plus polarized basis set was adopted for the valence electrons. The generalized gradient approximation proposed by Becke gradient exchange functional [22] and Lee, Yang, Parr correlation functional [23] was used to calculate the exchange-correlation term. The pseudopotentials were

E-mail address: murat.durandurdu@agu.edu.tr.

http://dx.doi.org/10.1016/j.jnoncrysol.2015.07.033
0022-3093/

generated using the Troullier–Martins scheme [24]. Γ-point was applied solely for the Brillouin zone integration. The molecular-dynamics (MD) simulations were done within the isothermal–isobaric ensemble. The velocity scaling technique was applied to control temperature. The Parrinelo–Rahman method [25] was used to equilibrate pressure but the shear deformations were not allowed. A MD time step of one femtosecond (fs) was used. *c*-BN was chosen as a starting structure with 108 B and 108N atoms. The structure was subjected to a high temperature of 5500 K for 2.0 ps. Then temperature was gradually reduced to 3300 K at which the structure was equilibrated for 10.0 ps. Finally, the liquid state was quenched to 300 K in 10.0 ps. The resulting amorphous structure was relaxed using the conjugate gradient technique. Its final density of the *a*-BN model was equal to 2.042 g/cm^3. The last 1000 MD steps of the liquid state were collected for the structural analyses. Some thermodynamic parameters during the quenching as a function of MD time were illustrated in Fig. 1. Based on the fluctuations of thermodynamic parameters at the liquid state due to the finite size of system, the uncertainty in these parameters is estimated to be less than 1.0% using the standard error analysis.

3. Results

The partial pair distribution functions (PPDFs) of the relaxed amorphous model are shown in Fig. 2. The strongest peak of the B–N, B–B and N–N pairs is located at 1.46 Å, 2.51 Å and 2.54 Å, respectively. Comparing this B—N bond length with that of two- and three-dimensional crystalline *h*-BN and *c*-BN phases, one can see that it is noticeably shorter than sp^3 bond distance of 1.57 Å (Ref. [26]) but comparable with sp^2 bond length of 1.44 Å (Ref. [26]). On the other hand, the position of the strongest B–B and N–N peak of *a*-BN is close to the second neighbor (B–B or N–N) separations of 2.50 Å for *h*-BN and 2.56 Å for *c*-BN (Ref. [26]). An important structural feature presented in the B–B and N–N pairs, which is not offered in the crystalline BNs, is the presence of weak peaks or subpeaks at the shorter correlation distances, signifying the existence of N—N and B—B bonds in *a*-BN. The weak peak around 1.47 Å in the N–N pair is not due to the N_2 dimer because the bond length of N_2 dimer is close to 1.1 Å. N atoms involving with the wrong bond are threefold coordinated. The subpeak around 1.70 Å in the B–B pair is due to the single B—B bond, creating a pentagonal ring in the amorphous network. The second subpeak/shoulder in both N–N

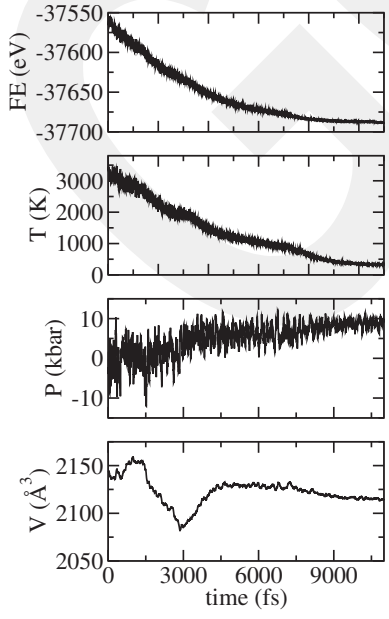

Fig. 1. Free energy (FE), temperature (T), pressure (P) and volume (V) as a function of MD time.

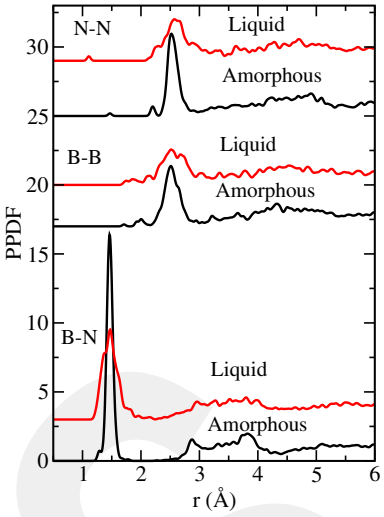

Fig. 2. PPDFs of the relaxed *a*-BN and liquid BN at 3300 ± 32 K.

(around 2.2 Å) and B–B (near 2.01 Å) correlations is not associated with homopolar bond(s) but they are due to the tetragonal BN rings (diamond shaped) as shown in Fig. 3. The tetragonal ring regularly forms in the BN nanocages [27,28] and hence it is not an unfamiliar cluster type for BN. Yet a surprising finding is that each tetragonal ring in *a*-BN is slightly deformed and the B–B correlation is always less than that of N–N separation. The most important conclusion derived from the PPDF analysis is the formation of negligible amount of homopolar bonds in *a*-BN unlike the earlier simulations [18,19].

The coordination number (CN) is a fundamental parameter describing the atomic structure of an amorphous network in details. The CN of *a*-BN is calculated using the cutoff distances of 1.89 Å for B–N, 1.81 Å for B–B and 1.64 Å for N–N. Fig. 4 shows the coordination distribution. The threefold-coordinated atoms are prevailed with a frequency of 91%. The fraction of twofold- and fourfold-coordinated atoms is rather unimportant and is about 6% and 3%, respectively. The resulting average CN is 2.97. We should stress here that not all sp^2 bonding form complete hexagonal rings, some generate the tetragonal or incomplete hexagonal ones and the rest plays a partial role for the formation of larger rings. The twofold coordinated atoms shape chain-like structures. The fourfold-coordinated atoms produce tetrahedrons and some of which are quite deformed with three bonds (~1.55 Å) and one longer one (~1.77 Å). Therefore their angles are quite off from the ideal tetrahedral angle of ~109.5°. All these findings support predominant sp^2 bonding in *a*-BN and further suggest the existence of sp bonding whose concentration is higher than that of sp^3 bonding.

For a deeper understanding of the microstructure of *a*-BN, we also study the bond angle distribution function (BADF). Its B–N–B and N–B–N angle distributions are given in Fig. 5. The model has very broad distributions with the main peak located around 120°, indicating that the *a*-BN has a strong tendency to attain a local structure similar to that of *h*-BN. The subpeak around 80° for the B–N–B and 95° for N–B–N are due to the tetragonal rings (see Fig. 3). The angles larger than 130° are mostly related to the chain-like clusters.

Since some of technological applications of BN depend on its electronic structure, we finally study the electronic density of state (EDOS) of *a*-BN and *h*-BN and show them in Fig. 6. *h*-BN has a band gap energy of around 4.5 eV, which is less than the experimental value of about 6.0 eV as expected due to the restriction of DFT to define the exited states. *a*-BN also presents a clear band gap energy whose magnitude is roughly 2.0 eV. This band gap energy is expected to have a greater value in experiments. To have additional information about the electronic structure of *a*-BN, we also calculate the partial density of states (PDOS) and give them in Fig. 6. The energy band levels around

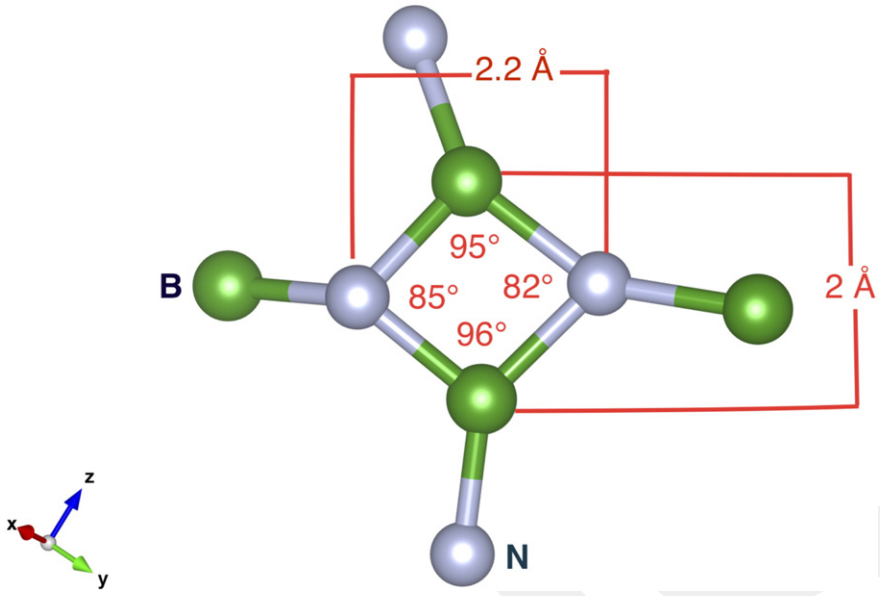

Fig. 3. Tetragonal ring formed in *a*-BN.

−20 eV have contributions from B-s, B-p and primarily N-s states. The upper valance band near the Fermi Level is due to B-s, B-p and mainly N-p states. The lower conduction band near the Fermi level is dominated by B-p states. Similar findings have been reported for *h*-BN in a first principles plane wave calculation [29].

4. Discussion

The computer generated *a*-BN model has primarily sp^2 bonding, which is consistent with the experiments [7,8] but it has neither N_2 dimers nor a considerable amount of homopolar bonds contrary to the earlier simulations [18,19]. Indeed the fraction of chemical disorder in the liquid BN is also very minor as shown in Fig. 2. The liquid BN at 3300 ± 32 K consists of single N_2 molecule as indicated by the weak peak located at 1.1 Å and two B—B wrong bonds. During the solidification process, one of B—B bonds and the N_2 molecule are purged around 1800 ± 17 K due to the structural rearrangements.

The contradictory findings in the simulations can be linked to many factors but we will focus on some important ones here to explain diverse observations. The first one is the size of simulation boxes. Our amorphous network (216 atoms) is fairly larger than the 64 and 140 atom models generated in the previous simulations [18,19]. For a larger system, indeed more homopolar bonds can be anticipated. Therefore the size cannot be a

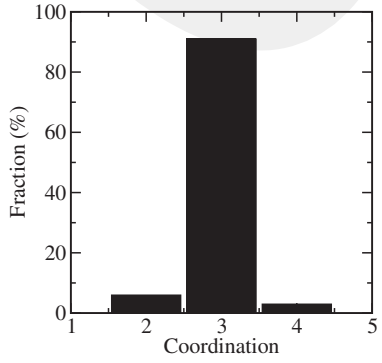

Fig. 4. Coordination distribution.

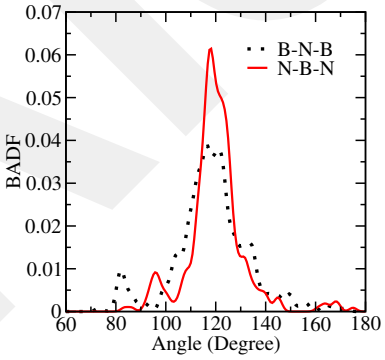

Fig. 5. BADF of *a*-BN.

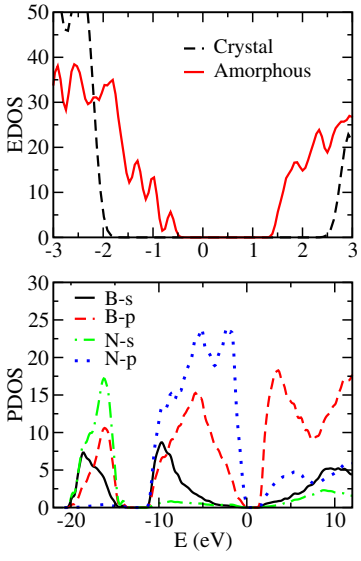

Fig. 6. EDOS for *h*-BN and *a*-BN (top panel) and PDOS for *a*-BN (bottom panel). Fermi level is at zero eV.

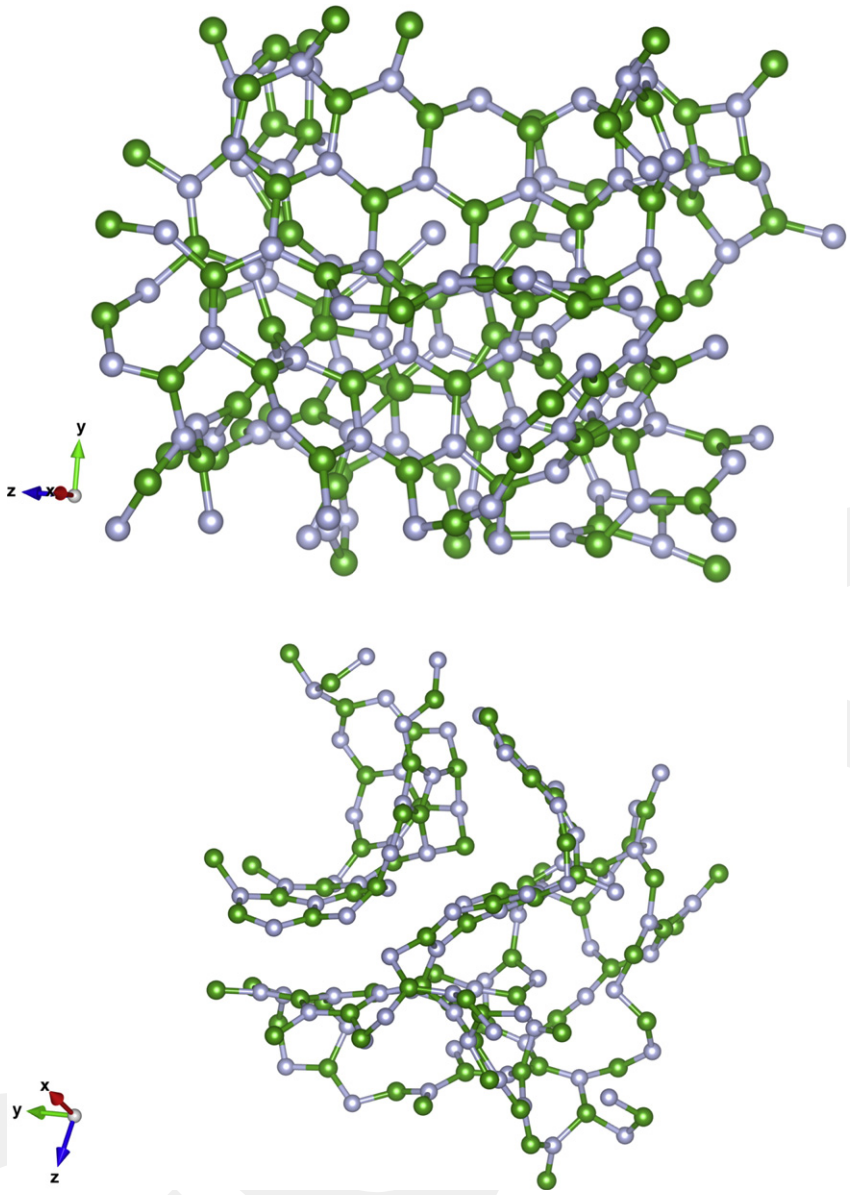

Fig. 7. Computer generated *a*-BN model. Dark atoms are B and light ones are N. For clarity, some atoms are removed from the model.

main reason for the dissimilar estimations. The second one is the simulation time. The total simulation time of the present work is quite longer than one used in the earlier studies and hence it can be an important factor for the inconsistent outcomes. In Ref. [18], a randomly arranged network was used as a starting structure, which was equilibrated for 1.0 ps at 10,000 K. This very high temperature state was quenched to 300 K in 2.0 ps. On the other hand, in Ref. [19], a highly unstable simple cubic state (it is initially very chemically disordered, see Fig. 2 of Ref. [19]) was chosen as an initial structure that was thermalized at 4000 K for 350 fs and cooled to 300 K in 500 fs. Therefore, we believe that the system in these simulations did not reach the true equilibrium state in short simulation times. Note that our starting structure was the ZB phase (4-fold coordinated), which is topologically very different than the most stable *h*-BN but a long simulation time resulted in an amorphous model whose local structural arrangement is close to that of *h*-BN.

Perhaps the most fascinating observation is the occurrence of randomly distributed some ordered geometries in the computer-generated model, which form hexagonal-like nanosheets as shown in Fig. 7. Therefore *a*-BN is not fully disordered but a mixture of ordered and disordered topologies, which probably explains why *a*-BN can easily transforms into turbostratic BN by thermal treatments [5]. Moreover the formation of tetragonal rings as in some BN nanocages and the bending of nanosheets might indicate that cage- or capsule-like nanostructures, perhaps uncompleted or very defective ones, can exist in *a*-BN as well. Consequently *a*-BN can have different types of nanostructures, which makes *a*-BN a unique material having different potential technological applications if their size and shape can be controlled or altered easily.

All these predictions, of course, are based on the simulation of a 216-atom model. For a larger system, different topological and chemical disorders can be anticipated. Indeed we expect slightly higher homopolar bonds, marginally more coordination defects (two and fourfold) and a larger scale of nanostructures in a bigger model. Since the physical properties depend on the morphology of the amorphous networks, any change in their topology and bonding will surely have some influences on them.

5. Conclusions

We have generated an *a*-BN model using an ab initio MD technique and analyze its atomic structure in details. The model is almost

chemically ordered and has predominantly sp^2 bonding which results in not only hexagonal rings but also tetragonal ones as seen in BN nanocages. The interconnecting hexagonal rings yield nanosheets and some of which are bended. The presence of tetragonal rings plus bending of nanosheets are interpreted as a possible formation of cage or capsule-like nanostructures in *a*-BN. The *a*-BN model possesses semiconducting properties.

Acknowledgment

This work was supported by the Scientific and Technical Research Council of Turkey (TÜBİTAK) under BİDEB-2232 program and grant no: 114C100.

References

[1] R.T. Paine, C.K. Narula, Synthetic routes to boron nitride, Chem. Rev. 90 (1990) 73–91.
[2] Y. Matsui, Y. Sekikawa, T. Sato, T. Ishii, S. Isakosawa, K. Shii, Formations of rhombohedral boron nitride, as revealed by TEM-electron energy loss spectroscopy, J. Mater. Sci. 16 (1981) 1114–1116.
[3] R.H. Wentorf Jr., Synthesis of the cubic form of boron nitride, J. Chem. Phys. 34 (1961) 809.
[4] F.P. Bundy, R.H. Wentorf Jr., Direct transformation of hexagonal boron nitride to denser forms, J. Chem. Phys. 38 (1963) 1144–1149.
[5] Ewan J.M. Hamilton, Shawn E. Dolan, Charles M. Mann, Hendrik O. Colijn, Clare A. McDonald, Sheldon G. Shore, Preparation of amorphous boron nitride and its conversion to a turbostratic, tubular form, Science 260 (1993) 659–661.
[6] H. Lorenz, I. Orgzall, In situ observation of the crystallization of amorphous boron nitride at high pressures and temperatures, Scr. Mater. 52 (2005) 537–540.
[7] R. Zedlitz, M. Heintze, M.B. Schubert, Properties of amorphous boron nitride thin films, J. Non-Cryst. Solids 198 (1996) 403–406.
[8] J.Y. Huang, H. Yasuda, H. Mori, HRTEM and EELS studies on the amorphization of hexagonal boron nitride induced by ball milling, J. Am. Ceram. Soc. 83 (2000) 403–409.
[9] S. Weissmantel, G. Reisse, B. Keiper, S. Schulze, Microstructure and mechanical properties of pulsed laser deposited boron nitride films, Diamond Relat. Mater. 8 (1999) 377–381.
[10] D.R. Ketchum, A.L. DeGraffenreid, P.M. Niedenzu, S.G. Shore, Synthesis of amorphous boron nitride from the molecular precursor ammonia-monochloroborane, J. Mater. Res. 14 (1999) 1934–1938.
[11] A. Werbowy, J. Szmidt, A. Sokolowska, A. Olszyna, S. Mitura, Fabrication and properties of Mo contacts to amorphous cubic boron nitride (a-cBN) layers, Diamond Relat. Mater. 5 (1996) 1017–1020.
[12] D. Li, C. Zhang, B. Li, F. Cao, S. Wang, K. Liu, Z. Fang, Low-cost preparation of boron nitride ceramic powders, J. Wuhan Univ. Technol. Mater. Sci. Ed. 27 (2012) 534–537.
[13] T. Taniguchi, K. Kimoto, M. Tansho, S. Horiuchi, S. Yamaoka, Phase transformation of amorphous boron nitride under high pressure, Chem. Mater. 15 (2003) 2744–2751.
[14] A. Werbowy, J. Szmidt, A. Sokołowska, A. Olszyna, Heterojunctions of amorphous wide band gap nitrides and silicon, Diamond Relat. Mater. 7 (1998) 397–401.
[15] K. Kayed, H. Abdeh, K. Alshoufi, Effect of nitrogen plasma after glow on amorphous boron nitride thin films deposited by laser ablation, Int. J. ChemTech Res. 6 (2014) 2719–2724.
[16] S.K. Singhal, J.K. Park, Cryst. synthesis of cubic boron nitride from amorphous boron nitride containing oxide impurity using Mg–Al alloy catalyst solvent, Cryst. Growth Des. 260 (2004) 217–222.
[17] F. Cao, K. Liu, Z. Fang, S. Wang, Hydrolysis mechanism of borazine-derived boron nitride pyrolysized below 1200 °C, J. Mater. Sci. Technol. 28 (2012) 956–960.
[18] J. Widany, Density-functional Tight-Binding Calculations on the Structure of Complex Boron Nitride Systems(PhD thesis) Technische Universität Chemnitz, Reichenhainer Straße 70, 09126 Chemnitz, Germany, 1997.
[19] D.G. McCulloch, D.R. McKenzie, C.M. Goringe, Ab initio study of structure in boron nitride, aluminum nitride and mixed aluminum boron nitride amorphous alloys, J. Appl. Phys. 88 (2000) 5028–5032.
[20] J.J. Pouch, S.A. Alterovitz, K. Miyoshi, J.O. Warner, Boron nitride: composition, optical properties, and mechanical behavior, MRS Proc. 93 (1987) 323.
[21] P. Ordejon, E. Artacho, J.M. Soler, Self-consistent order-N density functional calculations for very large systems, Phys. Rev. B 53 (1996) 10441–10444.
[22] A.D. Becke, Density-functional exchange energy approximation with correct asymptotic behavior, Phys. Rev. A 38 (1988) 3098–3100.
[23] C. Lee, W. Yang, R.G. Parr, Development of the Colle-Salvetti correlation-energy formula into a functional of the electron density, Phys. Rev. B 37 (1988) 785–789.
[24] N. Troullier, J.M. Martins, Efficient pseudopotentials for plane-wave calculations, Phys. Rev. B 43 (1991) 1993–2006.
[25] M. Parrinello, A. Rahman, Polymorphic transitions in single crystals: a new molecular dynamics method, J. Appl. Phys. 52 (1981) 7182–7190.
[26] Y. Kumashiro (Ed.), Electric Refractory Materials, Taylor & Francis, New York, 2000.
[27] H.S. Wu, X. Hong Xu, F.Q. Zhang, H. Jiao, New boron nitride B24N24 nanotube, J. Phys. Chem. A 107 (2003) 6609–6612.
[28] Hai-Shun Wu, Haijun Jiao, What is the most stable B24N24 fullerene? Chem. Phys. Lett. 386 (2004) 369–372.
[29] M. Topsakal, E. Aktürk, S. Ciraci, First-principles study of two- and one-dimensional honeycomb structures of boron nitride, Phys. Rev. B 79 (2009) 115442–115452.